ANTICANCER RESEARCH *26*: 2791-2804 (2006)

# Antiproliferative and Proapoptotic Activities of Pyranoxanthenones, Pyranothioxanthenones and their Pyrazole-fused Derivatives in HL-60 Cells

ELISABETH M. PERCHELLET[1], MARY M. WARD[1], ALEXIOS-LEANDROS SKALTSOUNIS[2], IOANNIS K. KOSTAKIS[3], NICOLE POULI[3], PANAGIOTIS MARAKOS[3] and JEAN-PIERRE H. PERCHELLET[1]

*[1]Anti-Cancer Drug Laboratory, Division of Biology, Ackert Hall, Kansas State University, Manhattan, KS 66506-4901, U.S.A; Divisions of [2]Pharmacognosy and [3]Pharmaceutical Chemistry, Department of Pharmacy, University of Athens, Panepistimiopolis-Zografou, Athens 15771, Greece*

**Abstract.** *Background: Synthetic pyranoxanthenones, pyranothioxanthenones and their pyrazole-fused derivatives, which bind to DNA, block the $G_2$ + M-phases of the cell cycle and inhibit the proliferation of ascitic and solid tumor cell lines in vitro, were tested for their ability to induce apoptosis in the HL-60 cell system. Materials and Methods: Various markers of tumor cell metabolism, apoptosis induction and mitochondrial permeability transition (MPT) were assayed in vitro to evaluate drug cytotoxicity. Results: All these compounds, and especially the pyrazole-fused pyranoxanthenones **7**, **8** and **10**, which were effective in the 3-5 μM range and were more potent than the pyranoxanthenones, reduced the proliferation of HL-60 cells at 2 and 4 days. These antitumor drugs inhibited DNA synthesis at 2 h in relation to their ability to block the cellular uptake of purine and pyrimidine nucleosides within 15 min. Internucleosomal DNA fragmentation, a late marker of apoptosis, was induced in a concentration-dependent manner by **7** and **10** at 24 h. Poly(ADP-ribose) polymerase-1 (PARP-1) cleavage, an early event required for cells committed to apoptosis, was detected within 12 h in HL-60 cells treated with **7** and **10**. In accord with the fact that the caspase cascade is responsible for PARP-1 cleavage, **7** and **10** induced the activities of initiator caspases-2 and -9 and effector caspase-3 within 9 h in HL-60 cells. The release of mitochondrial cytochrome c (Cyt c) was also detected within 9 h in HL-60 cells treated with **7** and **10**, consistent with the fact that Cyt c is the apoptotic trigger that activates caspase-9. However, **7** and **10** neither caused the rapid collapse of mitochondrial transmembrane potential, nor the mitochondrial swelling linked to MPT. Conclusion: Pyrazole-fused pyranoxanthenones are DNA-interacting antiproliferative drugs that do not directly target mitochondria in cell and cell-free systems to induce the intrinsic pathway of apoptosis.*

*Correspondence to:* J.-P. Perchellet, Anti-Cancer Drug Laboratory, Kansas State University, Division of Biology, Ackert Hall, Manhattan, KS 66506-4901, U.S.A. Tel: +1 785-532-7727, Fax: +1 785-532-6653, e-mail: jpperch@ksu.edu

*Key Words:* Pyranoxanthenones, pyranothioxanthenones, HL-60 cell proliferation, nucleoside transport, DNA synthesis and fragmentation, cytochrome *c*, caspases, poly(ADP-ribose) polymerase-1, apoptosis.

Many anticancer drugs activate apoptosis, while defective apoptotic signaling pathways contribute to the development of multidrug resistance (MDR). Since the clinical effectiveness of anticancer drugs that possess the anthracene-9,10-dione skeleton as part of their structure, such as doxorubicin, daunorubicin and mitoxantrone, may be limited by their cardiotoxicity and ability to induce MDR, it is important to develop quinone-free derivatives with improved bioactivity and determine whether apoptosis plays a decisive role in their molecular mechanism of action. The acridone alkaloid acronycine is a broad-spectrum antitumor agent with poor water solubility (1-4). Recently, we synthesized pyranoxanthenone and pyranothioxanthenone analogs of acronycine, which were more potent than the parent compound in inhibiting L1210 cell proliferation, but mimicked the ability of acronycine to block cell cycle progression in the $G_2$ + M-phase, suggesting that these drugs may share a similar molecular mechanism of action (5). Moreover, we incorporated a pyrazole ring fusion into the acridone and (thio)-xanthenone ring of the acronycine analogs to generate a new class of compounds bearing structural similarity to both acronycine and the anthrapyrazoles (6). Quinone-free anthrapyrazoles, resulting from a pyrazole ring fusion at the 1- and 9-positions of the tricyclic skeleton of mitoxantrone, exhibited increased antitumor activity and reduced cardiotoxicity (7). Our new pyrazole-fused pyranoxanthenone and pyranothioxanthenone derivatives interacted with DNA, as indicated by their ethidium bromide (EB) displacement potency and, besides

murine L1210 leukemia, were more effective than acronycine at inhibiting the proliferation of solid human tumor cell lines, including A549 lung, MDA-MB-231 breast, and HT-29, HCT-116 and HRT-18 colon cancer (6).

Because neoplastic cells undergoing apoptosis may be phagocytosed, novel pyranoxanthenones, pyranothioxanthenones and their pyrazole-fused derivatives (the most antiproliferative compounds that can induce apoptosis) might be valuable in developing new means of polychemotherapy. Drug-damaged tumor cells irreversibly committed to the apoptotic pathway exhibit mitochondrial dysfunction, cytoplasmic and nuclear condensation, plasma membrane blebbing, DNA degradation into oligonucleosomal fragments and packaging of cellular components into discrete membrane-bound apoptotic bodies that are rapidly phagocytosed by surrounding cells and macrophages. Whether death receptor-dependent or -independent, the different apoptosis signaling pathways induced by various anticancer drugs with distinct primary subcellular targets and mechanisms of action may converge on mitochondria to cause mitochondrial permeability transition (MPT), release apoptogenic factors from the mitochondrial intermembrane space (IMS) into the cytosol, activate a similar caspase proteolytic cascade that is amplified by a positive feedback loop involving the release of mitochondrial cytochrome *c* (Cyt *c*) and, ultimately, trigger internucleosomal DNA fragmentation (8, 9). Hence, the present study was undertaken to determine whether a selection of antitumor pyranoxanthenones, pyranothioxanthenones and their pyrazole-fused derivatives (5, 6) would trigger the sequential markers of apoptosis in HL-60 cells *in vitro*.

## Materials and Methods

*Cell cultures and drug treatments.* The synthesis of the pyranoxanthenones, pyranothioxanthenones and their pyrazole-fused derivatives under study have been reported (5, 6). All solutions of pyranoxanthenone and pyranothioxanthenone derivatives, synthetic 6-bromomethyl-1,4-anthracenedione (AQ9), carbonyl cyanide *m*-chlorophenylhydrazone (CCCP; from Sigma, St. Louis, MO, USA) and 5,5',6,6'-tetrachloro-1,1',3,3'-tetraethylbenzi-midazolylcarbocyanine iodide (JC-1 dye; Molecular Probes, Eugene, OR, USA) were dissolved and diluted in dimethyl sulfoxide, whereas mitoxantrone (Sigma) solutions were prepared in double-distilled water, and 2-(6-amino-3-imino-3*H*-xanthe-9-yl)benzoic acid methyl ester (Rh 123 dye, rhodamine 123) and alamethicin (both from Sigma) were formulated in 50% EtOH. The concentrations of these vehicles in the final incubation volumes never exceeded 0.2% and did not interfere with the data. Suspension cultures of human HL-60 promyelocytic leukemia cells (ATCC, Manassas, VA, USA) were maintained in continuous exponential growth in RPMI 1640 medium supplemented with 10% fetal bovine calf serum and penicillin (100 IU/ml)-streptomycin (100 μg/ml) and were incubated in the presence or absence (control) of drugs at 37˚C in a humidified atmosphere containing 5% $CO_2$ (10-13).

*Cell proliferation assay.* The growth of drug-treated HL-60 cells (initial densities $3x10^5$ cells/ml and $75x10^3$ cells/ml for 2- and 4-day long experiments, respectively) was assessed from their mitochondrial ability to bioreduce the 3-(4,5-dimethylthiazol-2-yl)-5-(3-carboxymethoxyphenyl)-2-(4-sulfophenyl)-2*H*-tetrazolium (MTS) reagent (Promega, Madison, WI, USA) in the presence of phenazine methosulfate (PMS; Sigma) into a water-soluble formazan product which absorbs at 490 nm (10, 12, 14). After 2 or 4 days at 37˚C in 48-well Costar culture plates, control and drug-treated cell samples (about $10^6$ cells/0.5 ml/well for controls) were further incubated at 37˚C for 3 h in the dark in the presence of 0.1 ml of MTS:PMS (2:0.1) reagent and their relative metabolic activity was estimated by recording the absorbance at 490 nm, using a Cambridge model 750 automatic microplate reader (Packard, Downers Grove, IL, USA) (10, 12, 14).

*Nucleoside transport and DNA synthesis.* HL-60 cells ($1.2x10^6$ cells/ml) were pre-incubated for 15 min at 37˚C in the presence or absence of drugs and were then exposed to 1 μCi of [2,8-$^3$H]adenosine (30 Ci/mmol; American Radiolabeled Chemicals, St. Louis, MO, USA) or [methyl-$^3$H]thymidine (50 Ci/mmol; Amersham, Arlington Heights, IL, USA) for only 30 sec to, respectively, assess the cellular uptake of purine and pyrimidine nucleosides over such a short period of time (10, 15). After diluting the reactions and washing three times with 2 ml of ice-cold $Ca^{2+}$/$Mg^{2+}$-free Dulbecco's phosphate-buffered saline (PBS) to remove the unincorporated radiolabel, cell pellets were harvested by centrifugation at 200 x g for 10 min and incubated for 30 min in 1 ml of hypotonic lysis buffer (HLB) containing 10 mM Tris-HCl, pH 8.0, 1 mM EDTA and 0.2% Triton X-100. The cell lysates were mixed with 6 ml of Bio-Safe II (Research Products International, Mount Prospect, IL, USA) to estimate the cellular uptake of [$^3$H]adenosine or [$^3$H]thymidine by liquid scintillation counting (LSC) (10, 15). To estimate the rate of DNA synthesis, $10^6$ HL-60 cells/ml were incubated at 37˚C for 90 min in the presence or absence of drugs and then pulse-labeled for an additional 30 min with 1 μCi of [$^3$H]thymidine (10, 15). After stopping the incubations with 0.5 ml of 10% trichloroacetic acid (TCA) and holding on ice for 15 min, the acid-insoluble material was recovered over Whatman GF/A glass microfiber filters and washed three times with 2 ml of 5% TCA and twice with 2 ml of 100% EtOH. After drying the filters, the radioactivity bound to the acid-precipitable material was determined by LSC in 6 ml of Bio-Safe NA (Research Products International) (10, 15).

*Detection of DNA fragmentation.* Drug-induced DNA cleavage was determined by intact chromatin precipitation, using HL-60 cells which were prelabeled with 1 μCi of [$^3$H]thymidine for 2 h at 37˚C, washed with 3 x 1 ml of ice-cold PBS, collected by centrifugation, resuspended in fresh medium at a density of $1.2x10^6$ cells/ml, and then incubated at 37˚C for 24 h in the presence or absence of drugs (10, 12, 15). After centrifugation at 200 xg for 10 min to discard the drugs and wash the cells, the cell pellets were lysed for 20 min in 0.5 ml of ice-cold HLB and centrifuged at 12,000 xg for 15 min to collect the supernatants. The radioactivity in the supernatants (detergent-soluble low molecular weight DNA fragments) and the pellets (intact chromatin DNA) was determined by LSC. Before being counted in 6 ml of Bio-Safe NA, the intact pelleted chromatin was incubated for 2 h at 60˚C in the presence of 0.6 ml of NCS tissue solubilizer (Amersham) (10, 12, 15). For internucleosomal DNA fragmentation, HL-60 cells were incubated at 37˚C for 24 h in the presence or absence of drugs and DNA was extracted from samples

with equal cell densities ($2x10^6$ cells/ml), using a salting out procedure (12, 15). The cell pellets were washed twice with PBS, lysed overnight at 37˚C in 0.34 ml of 10 mM Tris-HCl, pH 8.0, containing 2 mM EDTA, 400 mM NaCl, 1% SDS and proteinase K (0.5 mg/ml), vortexed for 15 sec with 0.1 ml of 6 M NaCl and centrifuged (2,500 xg for 30 min) and the DNA was precipitated from the supernatants (0.44 ml) with 0.88 ml of 100% EtOH for 15 min at 4˚C. After centrifuging (14,000 xg for 15 min) at 4˚C, the air-dried DNA pellets were dissolved in 0.34 ml of 10 mM Tris-HCl, pH 8.0, with 1 mM EDTA (TE buffer) and incubated for 2 h at 37˚C in the presence of RNase (0.1 mg/ml). After another round of EtOH precipitation and centrifugation, the final air-dried pellets were dissolved in 50 μl of TE buffer and their DNA concentrations determined spectrophotometrically at 260 nm. Equal amounts of DNA samples (6 μg/7.5 μl TE buffer) were mixed with 1.5 μl of 10 mM Tris-HCl, pH 7.5, containing 50 mM EDTA, 10% Ficoll 400 and 0.4% Orange G, and loaded on each lane. About 0.5 μg of 100 bp DNA ladder and 0.75 μg of λ DNA/*Eco*RI + *Hind*III (both from Promega) were similarly applied to each gel to provide size markers in the range 100 to 1,500 and 125 to 21,226 bp, respectively. Horizontal electrophoresis of the DNA samples was performed for 3.7 h at 60 V in 1.5% agarose gels containing EB (1 μg/ml) with 90 mM Tris-HCl, pH 8.0, containing 90 mM boric acid and 2 mM EDTA as a running buffer. The DNA fragments were visualized and photographed with Polaroid 667 film under UV light at 312 nm, using a FisherBiotech model 88A variable-intensity UV transilluminator (12, 15).

*Fluorogenic assay of caspase activities.* Control and drug-treated HL-60 cells ($10^6$/ml) were incubated for 9 h at 37˚C, collected by centrifugation at 200 xg for 10 min, and washed with 1 ml of ice-cold PBS. The cell pellets were resuspended in chilled 10 mM Hepes buffer, pH 7.4, containing 100 mM NaCl, 100 mM KCl, 5 mM $MgCl_2$, 1 mM EDTA, 10 mM EGTA, 10% sucrose, 1 mM phenylmethylsulfonyl fluoride (PMSF), 1 mM dithiothreitol (DTT) and 100 μM digitonin (175 μl for caspase-3 assay and 120 μl for caspase-2 and -9 assays) and were lysed for 10 min on ice. The cell lysates were centrifuged at 14,000 xg for 20 min at 4˚C to precipitate cellular debris and the supernatants were stored at –70˚C overnight (12, 14). The caspase-2-, -9- and -3-like activities of the lysates were determined in reaction mixtures that contained 50 μl of lysis buffer (blank) or supernatant (control or drug-treated samples) and 50 μl of reaction buffer (100 mM Hepes, pH 7.5, containing 1 mM EDTA, 10 mM EGTA, 10% sucrose and 10 mM DTT), that were initiated by the addition of 5-μl aliquots of the respective 5 mM benzyloxycarbonyl (z)-Val-Asp-Val-Ala-Asp (VDVAD)-7-amino-4-trifluoromethylcoumarin (AFC), 5 mM acetyl-Leu-Glu-His-Asp (Ac-LEHD)-AFC or 1 mM z-Asp-Glu-Val-Asp (DEVD)-AFC stocks of AFC-substrate conjugates (all from Calbiochem, La Jolla, CA, USA) (12, 14). After incubation for 1 h at 37˚C in 96-well Costar white opaque polystyrene assay plates, the fluorescence of the free AFC released upon proteolytic cleavage of the substrate by the appropriate caspase was detected at 400-nm excitation and 505-nm emission, using a Cary Eclipse Fluorescence Spectrophotometer equipped with a microplate reader accessory (Varian, Walnut Creek, CA, USA). Arbitrary fluorescence units were quantified with reference to calibration curves ranging from 0.01 to 6 nmol of AFC (from Sigma), the protein concentrations of the supernatants were determined using the BCA Protein Assay Kit (Pierce, Rockford, IL, USA) and the VDVAD-, LEHD- and DEVD-specific cleavage activities of the samples were expressed as nmol of AFC released/mg of protein (12, 14).

*Western blot analysis of poly(ADP-ribose) polymerase-1 (PARP-1) cleavage and Cyt c release.* Suspensions of control and drug-treated HL-60 cells ($1.3x10^6$ cells/ml) were incubated for 12 or 9 h at 37˚C in 15 mm x 60 mm Petri dishes containing final volumes of 4.5 or 5 ml for PARP-1 or Cyt *c* analysis, respectively. For PARP-1 cleavage, $5.85x10^6$ tumor cells were collected by centrifugation, washed with 1 ml of PBS, lysed with 75 μl of 50 mM Tris-HCl buffer, pH 6.8, containing 250 mM NaCl, 1 mM $CaCl_2$, 50 mM NaF, 0.1% Triton X-100, 6 M urea and protease inhibitors (10 μg leupeptin/ml, 8 μg aprotinin/ml, 1 mM PMSF and the complete EDTA-free protease inhibitor cocktail from Roche Diagnostics Corp., Indianapolis, IN, USA), and disrupted by sonication with a tapered microtip for 12 strokes at power level 4 (80% duty cycle), using a 250 W Vibra Cell Ultrasonic Processor (Sonics & Materials, Danbury, CT, USA) (11, 12). For Cyt *c* release, pellets of $6.5x10^6$ PBS-washed cells were lysed for 30 min on ice with 80 μl of 10 mM Hepes buffer, pH 7.4, containing 100 mM NaCl, 100 mM KCl, 5 mM $MgCl_2$, 1 mM EDTA, 10 mM EGTA, 1 mM DTT, 10% sucrose, 1 mM PMSF, 0.2 mg leupeptin/ml, 0.2 mg aprotinin/ml and 100 μM digitonin (12, 14). The cell lysates were centrifuged at 14,000 xg for 15 min and the protein concentrations of the cytosolic supernatants were determined with the BCA Protein Assay Kit. For PARP-1 cleavage, aliquots of supernatants containing equal 70-μg quantities of proteins were incubated with SDS sample loading buffer (final concentration 10% glycerol, 2% SDS, 5% β-mercaptoethanol, 0.02% bromophenol blue) for 15 min at 65˚C, resolved by electrophoresis for 50 min at 175 V in a 8% SDS-polyacrylamide gel, and transferred for 90 min to a PVDF sequencing membrane (Immobilon-P$^{SQ}$; Millipore, Bedford, MA, USA) using a Panther model HEP1 Semidry Electroblotter (Owl Separation Systems, Portsmouth, NH, USA) (11, 12). For Cyt *c* release, aliquots of supernatants containing equal 100-μg amounts of proteins were boiled for 5 min in SDS sample loading buffer, resolved by electrophoresis for 75 min at 110 V in a 15% SDS-polyacrylamide gel and transferred for 1 h to the above PVDF sequencing membrane (12, 14). The blots were blocked with 5% nonfat dry milk in 20 mM Tris-HCl buffer, pH 7.4, with 0.9% NaCl (TBS), containing 0.05% of Tween-20 (TBST) for 90 min at room temperature. Immunodetections of PARP-1, Cyt *c* or β-actin were conducted at 4˚C overnight in TBST containing 2% of nonfat dry milk using, respectively, 0.5 μg/ml of mouse anti-PARP-1 (Ab-2) primary monoclonal antibody (mAb) (C-2-10; Calbiochem), which recognizes both the full-length 115 to 116-kDa native PARP-1 protein and its 85 to 90-kDa cleavage fragment (11, 12), 1 μg/ml of mouse anti-Cyt *c* (7H8.2C12) primary mAb (BD PharMingen, San Diego, CA, USA), which recognizes the 15-kDa denatured form of Cyt *c* (12, 14, 16), or anti-β-actin (AC-15) primary mAb (1:15,000 dilution; Sigma), which recognizes an epitope located on the N-terminal end of the β-isoform of actin in a wide variety of tissues and species. After the blots had been rinsed three times with TBST, incubated for 1 h at room temperature in TBST containing 2% of nonfat dry milk and goat anti-mouse secondary mAb conjugated with horseradish peroxidase (1:30,000 dilution; Oncogene, Boston, MA, USA) and rinsed again three times with TBST, Kodak BioMax light film was used to develop images of the immunoreactive bands revealed by enhanced chemiluminescence (CL) staining, using the SuperSignal West Pico CL Substrate (Pierce). The integrated density values of the Western blots were compared by digital image analysis (Chemi Imager 5500 with AlphaEase FC™ software), using a MultiImage Light Cabinet (Alpha Inotech, San Leandro, CA, USA) (11, 12, 14). Detection of the 42-kDa band of β-actin was performed as an internal control to confirm equal protein loading.

*Mitochondrial depolarization assay in HL-60 cells.* The JC-1 dye is used to detect the collapse (↓) of mitochondrial transmembrane potential (Δψm) in drug-treated cells because its Δψm-dependent accumulation and fluorescence emission shift are more specific for mitochondrial than plasma membrane potential (17, 18). At high Δψm, JC-1 is internalized and concentrated at the mitochondrial inner membrane (IM) to form micelle-like J-aggregates, which dissociate at lower Δψm to become free JC-1 monomers. Since J-aggregates emit a longer wavelength than JC-1 monomers, the sudden decrease in the JC-1 fluorescence emission ratio of red aggregates/green monomers was detected at 595/535 nm to demonstrate the ↓Δψm in drug-treated HL-60 cells (13, 17, 18). Control or drug-treated tumor cells ($0.5x10^6$/ml) were preincubated in 1.5-ml Eppendorf tubes for 10 min at 37˚C before being loaded for 30 min with 1 μl of fluorescent dye to obtain a final concentration of 0.3 μM JC-1. After centrifuging (200 xg for 5 min) and washing at room temperature to discard the drugs and unincorporated free dye, the fluorescence readings of the resuspended cell pellets were stabilized for 20 min at 37˚C. After transferring 0.2-ml aliquots of these incubates to a 96-well Costar white opaque polystyrene assay plate, the decreased JC-1 fluorescence ratio of red aggregates/green monomers linked to the ↓Δψm was immediately detected at 490 nm excitation and 595/535 nm emission, using a Cary Eclipse Fluorescence microplate reader (13).

*Depolarization and swelling assays in isolated mitochondria.* Mitochondria were isolated by differential centrifugation at 4˚C from one female CF-1 (Charles River, Wilmimgton, MA, USA) mouse liver after an overnight period of fasting to deplete the levels of glycogen and fatty acids (13, 19, 20). The liver was rinsed, minced with scissors and homogenized in 40 ml of 10 mM Hepes buffer, pH 7.2, containing 225 mM mannitol, 75 mM sucrose, 1 mM EGTA and 0.1% bovine serum albumin, with two slow up/down strokes of a motorized tight-fitting Teflon pestle rotating at about 500 rpm in a glass Potter-Elvejhem tissue grinder. The disrupted cells were centrifuged (1,000 xg for 10 min) to precipitate unlysed cells, nuclei and large membrane fragments. The supernatant was decanted and then recentrifuged (10,000 xg for 10 min) to collect the mitochondrial pellets, which were washed, pooled and resuspended at a final concentration of 50 mg protein/ml of 10 mM Hepes buffer, pH 7.2, containing 225 mM mannitol and 75 mM sucrose (13, 19, 20). The protein concentrations of the mitochondrial samples were determined using the BCA Protein Assay Kit.

The Rh 123 dye is a sensitive and specific probe of Δψm in isolated mitochondria because its retention or release is dependent on the maintenance or loss of Δψm across the IM (21). The red shift in the excitation and emission spectra and the energy-dependent quenching of Rh 123 fluorescence intensity, which occur upon Δψm-driven dye uptake, binding into the matrix space and redistribution across the polarized IM of coupled mitochondria, are then rapidly and fully reversed when this fluorescent probe is released by uncoupled mitochondria following de-energization and ↓Δψm (21). To assay the ↓Δψm in isolated mitochondria, 1.5-ml Eppendorf tubes were sequentially supplemented with 1 ml of mitochondrial reaction buffer (MRB), containing 10 mM Hepes, pH 7.2, 100 mM sucrose, 65 mM KCl, 5 mM glutamate, 2.5 mM malate, 1 mM $KH_2PO_4$ and 20 μM EGTA, 4 μl of fluorescent dye to obtain a final concentration of 1 μM Rh 123, and 10 μl of isolated mitochondria (0.5 mg of protein). After incubation of these control and drug-treated reaction mixtures for 5 min at room temperature, 0.2-ml aliquots were transferred to a 96-well Costar white opaque polystyrene assay plate and the unquenched fluorescence of the Rh 123 dye, which is released from mitochondria and indicative of the ↓Δψm, was monitored for 30 min at 503 nm excitation/525 nm emission, using a Cary Eclipse Fluorescence microplate reader (13, 21).

Opening of the mitochondrial permeability transition pore (PTP) triggers a sudden and non-specific permeabilization of the IM to ions and solutes and the hyperosmolarity of the matrix induces $H_2O$ to enter from the cytosol and cause rapid mitochondrial swelling, which is a true marker of MPT. Conventional rod-shaped mitochondria are packed with small and dense cristae, whereas large and swollen mitochondria have diluted matrices with cristae in various stages of disintegration. Since severely swollen mitochondria with clear matrices and disrupted cristae scatter and absorb much less light than the dense and granular light-absorbing structures of their normal compact counterparts, a decrease in light scattering reflects the degree of mitochondrial swelling (22, 23). Hence, the large amplitude swelling of mitochondria undergoing drug-induced MPT was determined spectrophotometrically by monitoring the decrease in apparent absorbance (light-scattering) at 540 nm (20, 22, 23). To assay mitochondrial swelling, 24-well Costar clear transparent polystyrene cell culture plates were sequentially supplemented with 1 ml of MRB and 10 μl of isolated mitochondria (0.5 mg of protein). After incubation of these control or drug-treated reaction mixtures for 5 min at room temperature, the decrease of absorbance (light-scattering) linked to large amplitude mitochondrial swelling was monitored for 30 min at 540 nm, using a Cambridge model 750 automatic microplate reader. The data of all biochemical experiments were analyzed using the Student's *t*-test with the level of significance set at $p<0.05$.

## Results

*Inhibition of HL-60 cell proliferation.* The chemical structures and numbers of the synthetic pyranoxanthenones, pyranothioxanthenones and their pyrazole-fused derivatives, tested for their antitumor and apoptotic activities in the HL-60 cell system *in vitro,* are depicted in Figure 1. The method for synthesizing these antitumor agents as analogs of the acridone alkaloid acronycine, their nomenclature and their ability to bind to DNA, block cell cycle progression in the $G_2$ + M-phases and inhibit the proliferation of murine L1210 leukemic cells and solid human A549, MDA-MB-231, HT-29, HCT-116 and HRT-18 tumor cell lines have been reported (5, 6). All compounds tested inhibited the mitochondrial ability of these HL-60 human leukemia cells to metabolize the MTS:PMS reagent at days 2 and 4 (Figure 1). Compounds **2**, **4**, **10** and **11** are representative examples of pyranoxanthe-nones, pyranothioxanthenones, pyrazole-fused pyranoxanthenones and pyrazole-fused pyranothioxanthenones that inhibited HL-60 cell proliferation in the low μM range *in vitro* (Figure 1). The pyranoxanthenones **4**, **5**, **3** and **2** were generally less potent than their pyrazole-fused pyrano-xanthenone derivatives **6**, **11**, **7** and **8** (Figure 1). For instance, the concentration-dependent inhibitions of HL-60 tumor cell growth by the pyrazole-fused pyranoxanthenones **10** and **11** started at 1.6 μM and were maximal at 10 to 25 μM, whereas the antiproliferative effects of the pyranoxanthenones **2** and **4**

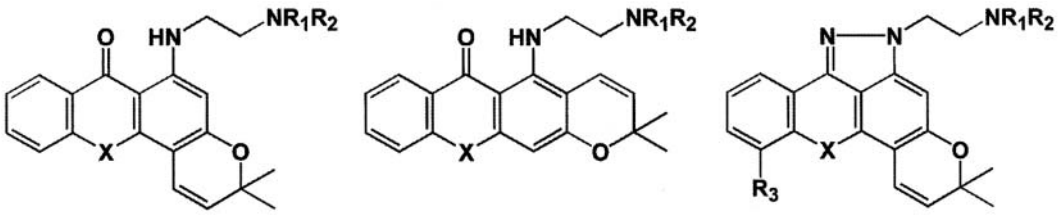


| | Compounds | | | $IC_{50}$ values (μM) in HL-60 cells | |
|---|---|---|---|---|---|
| Number | X | $NR_1R_2$ | R3 | at day 2 | at day 4 |
| **1** | S | $N(CH_3)_2$ | H | 188.9±9.3 | 85.2±4.2 |
| **2** | O | $N(CH_3)_2$ | H | 15.0±1.4 | 10.4±1.0 |
| **3** | O | $N(CH_2CH_3)_2$ | H | 100.4±6.8 | 71.8±7.9 |
| **4** | S | $N(CH_2)_4$ | H | 31.7±3.4[a] | 24.2±2.8[a] |
| **5** | S | $N(CH_2)_5$ | H | 55.5±2.1 | 40.7±3.6 |
| **6** | S | $N(CH_2)_4$ | H | 23.4±1.9[b] | 14.9±1.3[c] |
| **7** | O | $N(CH_2CH_3)_2$ | H | 4.8±0.3 | 3.1±0.3 |
| **8** | O | $N(CH_3)_2$ | H | 5.2±0.3[d] | 3.5±0.2[d] |
| **9** | O | $N(CH_2)_5$ | H | 8.2±0.6[e] | 6.1±0.5[f] |
| **10** | O | $N(CH_2)_4$ | H | 4.5±0.3[g] | 3.1±0.1[g] |
| **11** | S | $N(CH_2)_5$ | H | 10.6±0.6 | 4.4±0.5 |
| **12** | O | $N(CH_2CH_3)_2$ | $OCH_3$ | 6.1±0.4[h] | 3.5±0.2[i] |
| **13** | O | $N(CH_3)_2$ | $OCH_3$ | 6.6±0.4[j] | 4.0±0.4[k] |
| Mitoxantrone | | | | 0.0188±0.0009 | 0.0025±0.0002 |

Figure 1. *Chemical structures, numbers and concentrations of the synthetic pyranoxanthenones, pyranothioxanthenones and their pyrazole-fused derivatives required to inhibit by 50% ($IC_{50}$) the metabolic activity of human HL-60 tumor cells, using the MTS:PMS assay at days 2 and 4 in vitro. Tumor cell proliferation results (means±SD, n=3) were expressed as a % of the net absorbance of MTS/formazan after bioreduction by vehicle-treated control tumor cells (100±5%) after 2 ($A_{490\ nm}$=1.190±0.056) and 4 days ($A_{490\ nm}$=1.363±0.071) in culture. Blank values ($A_{490\ nm}$=0.318 and 0.357 at days 2 and 4) for cell-free culture medium supplemented with MTS:PMS reagent were substracted from the results. $IC_{50}$ values were calculated from linear regression of the slopes of the log-transformed concentration-survival curves. [a]p<0.005, less than **5**; [b]p<0.025 and [c]p<0.01, less than **4**; [d]p<0.0005, less than **2**; [e]p<0.01, less than **11** at day 2 but [f]p<0.025, more than **11** at day 4; [g]p<0.0005, less than **6**, not different from **7**, p<0.05, less than **8**, and p<0.005, less than **9**; [h]p<0.025, more than **7** at day 2 but not different from **7** at day 4; [j]p<0.01, more than **8** at day 2 but not different from **8** at day 4.*

started only at 4 to 10 μM and become maximal at 25 to 62.5 μM (Figure 2). Except for **9** and **11**, which had similar antiproliferative activity, pyranothioxanthenones in which the nitrogen atom of acronycine had been replaced by a sulfur atom were less effective than the pyranoxanthenones in which an oxygen atom occupied this position (Figure 1). For example, the O-containing skeletons of **2** and **10** had five to twelve times more antitumor activity than their respective S-containing analogs **1** and **6** (Figure 1). Comparative $IC_{50}$ values also indicated that $N(CH_3)_2$-substituted **2** was 7 times more bioactive than its $N(CH_2CH_3)_2$-substituted **3** analog. The $N(CH_2)_4$-substituted **4** and **10** showed two times more antiproliferative activity than their respective $N(CH_2)_5$-substituted **5** and **9** analogs (Figure 1). Moreover, the antitumor effects of **7** and **8** were not improved by a methoxy function in their respective derivatives, **12** and **13** (Figure 1). In any case, **7**, **8** and **10**, which were consistently the most potent against HL-60 cell proliferation at days 2 and 4 (Figure 1), were retained to study the markers of apoptosis induced by pyrazole-fused pyranoxanthenones in cell and cell-free systems. However, these lead antiproliferative pyranoxanthenone derivatives fell far from matching the potency of the reference anticancer drug mitoxantrone (Figure 1).

*Inhibition of DNA synthesis and nucleoside transport.* A 90-min treatment with pyrazole-fused pyranoxanthenones was sufficient to maximally inhibit the incorporation of [$^3$H]thymidine into DNA used to assess the rate of DNA synthesis over a 30-min period of pulse-labeling in HL-60 cells *in vitro* (Figure 3). The concentration-dependent inhibitions of DNA synthesis by **7** ($IC_{50}$: 4.7 μM) and **10** ($IC_{50}$: 4.1 μM) were nearly identical (Figure 3A) and suggested that these compounds prevented HL-60 cells from synthesizing DNA at 2 h in relation to their antiproliferative activities ($IC_{50}$: 4.8 and 4.5 μM for **7** and **10**) at day 2 (Figure 1). The link between these two antitumor effects

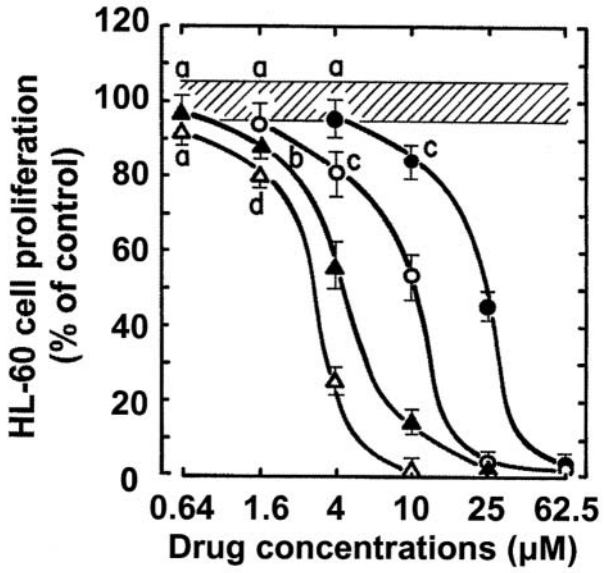


Figure 2. *Comparison of the abilities of serial concentrations (plotted on a logarithmic scale) of* ***2*** *(○),* ***4*** *(●),* ***10*** *(△) and* ***11*** *(▲) to inhibit the metabolic activity of HL-60 cells after 4 days in vitro. Tumor cell proliferations were assayed with the MTS:PMS reagent and expressed as a % of the controls (untreated tumor cells – blank: 100±5%, striped area). Bars: means±SD (n=3). [a]Not different from control; [b]p<0.05 and [c]p<0.025, less than control; [d]p<0.05, less than 1.6 μM* ***11****.*

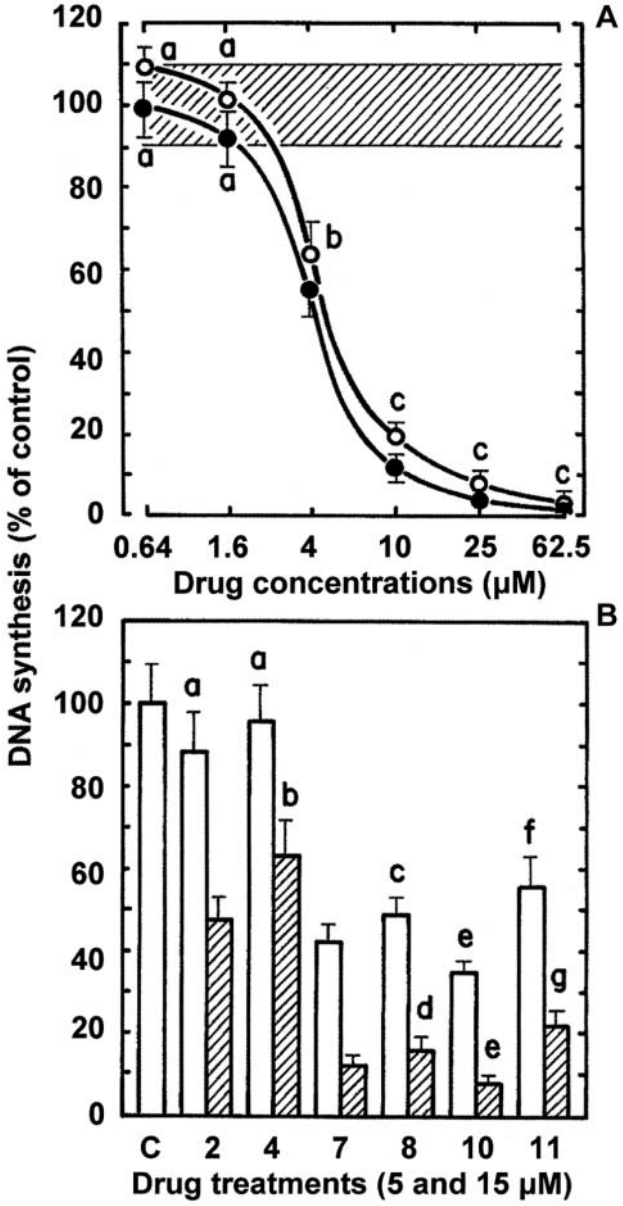


Figure 3. *Pyranoxanthenones, pyranothioxanthenones and their pyrazole-fused derivatives inhibited DNA synthesis in HL-60 cells. A) Comparison of the abilities of serial concentrations (plotted on a logarithmic scale) of* ***7*** *(○) and* ***10*** *(●) to inhibit the rate of incorporation of [3H]thymidine into DNA measured in HL-60 cells over 30 min following a 1.5-h period of incubation at 37˚C in vitro. DNA synthesis in vehicle-treated control cells at 37˚C was 16.231±1.574 cpm (100±9.7%, striped area). The blank value (493±39 cpm) for control cells incubated and pulse-labeled at 2˚C with 1 μCi of [3H]thymidine has been substracted from the results. Bars: means±SD (n=3). [a]Not different from control; [b]p<0.01, less than control but not different from* ***10****; [c]not different from* ***10****. B) Comparison of the abilities of 5 (open columns) and 15 μM (striped columns) concentrations of* ***2****,* ***4****,* ***7****,* ***8****,* ***10*** *and* ***11*** *to inhibit DNA synthesis in HL-60 cells at 2 h. C: control (untreated tumor cells – blank: 100±9.7%). [a]Not different from control; [b]p<0.01, less than control but p<0.05, more than* ***2****; [c]not different from* ***7*** *but p<0.01, more than* ***10****; [d]not different from* ***7*** *but p<0.025, more than* ***10****; [e]not different from* ***7****; [f]not different from* ***8****, but p<0.01, less than* ***2****; [g]not different from* ***8*** *but p<0.005, less than* ***2****.*

was substantiated by the fact that representative pyranoxanthenones, pyranothioxanthenones and their pyrazole-fused derivatives all inhibited DNA synthesis at 2 h (Figure 3B) compared to their antiproliferative potencies at day 2 (Figure 1). The pyranoxanthenones **2** and **4** were weaker than the pyrazole-fused pyranoxanthenone derivatives **7**, **8**, **10** and **11**.

Interestingly, a 15-min treatment with **7** or **10** was sufficient to block, in a concentration-dependent manner, the cellular uptake of [$^3$H]adenosine ($IC_{50}$: 4.4 and 7.8 μM for **7** and **10**) and [$^3$H]thymidine ($IC_{50}$: 3.5 and 5.3 μM for **7** and **10**) occuring over only 30 sec in HL-60 cells *in vitro* (Figure 4A). Representative pyranoxanthenones, pyranothioxanthenones and their pyrazole-fused derivatives all shared this ability to inhibit the cellular uptake of both purine and pyrimidine nucleosides at 15 min (Figure 4B) compared to their potencies against DNA synthesis at 2 h (Figure 3B) and tumor cell proliferation at 2 days (Figure 1). The pyranoxanthenones **2** and **4** were, again, observed to be weaker than the pyrazole-fused pyranoxanthenone derivatives **7**, **8**, **10** and **11**. Taken together, these results suggest that antitumor pyranoxanthenones may decrease the incorporation of radiolabeled nucleosides into DNA at 2 h (Figure 3) because they rapidly prevented the nucleoside transport system from incorporating these radiolabeled nucleosides into the HL-60 cells within 15 min (Figure 4).

*Induction of DNA fragmentation.* The abilities of antitumor pyranoxanthenone derivatives to induce internucleosomal DNA fragmentation at 24 h were demonstrated by two different techniques, using HL-60 cells containing [$^3$H]thymidine-prelabeled DNA to detect low molecular weight DNA fragments after intact chromatin precipitation (Figure 5) or agarose gel electrophoresis to visualize the typical pattern of DNA laddering indicative of apoptosis (Figure 6). The concentration-dependent inductions of DNA cleavage caused by **7** and **10** in HL-60 cells at 24 h started at 1.6 μM and peaked, respectively, 18.2 and 53.4% above control level (3.8% DNA fragmentation) at 10 and 25 μM before declining towards the control % of DNA fragmentation at the higher 25 and 62.5 μM concentrations, respectively (Figure 5A). Compared to the 15-fold response caused by 25 μM **7**, the fact that a lower 5.8-fold peak of DNA fragmentation was induced by a lower 10 μM concentration of **10** suggests that this compound may be more cytotoxic than **7** (Figure 5A). About the same increase and decrease of internucleosomal DNA fragmentation was confirmed by agarose gel electrophoresis of DNA samples extracted after 24 h from HL-60 cells treated with increasing concentrations of **7**, **8** and **10** (Figure 6). Compared to the controls, DNA cleavage bands with a characteristic pattern of internucleosomal ladders became increasingly visible in response to 1.6 to 4 μM concentrations of these compounds, peaked at 10 to 25 μM and then almost totally disappeared in response to 62.5 μM **7**, **8** and **10**, presumably because the higher concentrations of these antiproliferative drugs became so cytotoxic as to block the molecular events required to sustain the active process of apoptotic DNA fragmentation (Figure 6). Representative pyranoxanthenones, pyranothioxanthenones and their pyrazole-fused derivatives were all capable of inducing internucleosomal DNA fragmentation at 24 h (Figure 5B) compared to their antiproliferative activity at 2 days (Figure 1). Again, on an equimolar concentration basis and with the exception of **11**, the pyranoxanthenones **2** and **4** induced DNA fragmentation less effectively than 25 μM **7** and **8** and 10 μM **10** (Figure 5B), the latter compound being the most cytostatic of these pyrazole-fused pyranoxanthenone derivatives.

*Induction of PARP-1 cleavage.* The concentration-dependent effects of the antitumor pyrazole-fused pyranoxanthenone derivatives were assessed in HL-60 cells at 12 h, the first time at which **10** fully induced PARP-1 cleavage and the disappearance of the 116-kDa band of the native enzyme. Hence, there was no PARP-1 cleavage in untreated control cells but the band of the 85-kDa fragment became increasingly apparent 12 h after treatment with increasing 1.6 to 10 μM concentrations of **7** and **10** (Figure 7). In contrast to necrotic cells, which contain large amounts of uncleaved PARP-1 (24), virtually no intact PARP-1 was left after 12 h in apoptotic cells treated with 10 μM **10**, as indicated by the nearly total disappearance of the 116-kDa band of the native enzyme (Figure 7). However, based on the substantial intensity of the 116-kDa remnant and the smaller band of the 85-kDa fragment, PARP-1 was cleaved to a lesser degree by the same increasing concentrations of **7**, which only produced partial effects up to 10 μM (Figure 7). This is in accord with the finding that apoptotic DNA fragmentation peaked at 10 μM **10,** but was only partially induced by 10 μM **7** (Figure 5).

*Activation of initiator and effector caspases.* Since the degradation of PARP-1 is catalyzed by caspase-3, the key downstream effector caspase proteolytically activated by the initiator caspase-9, the pyrazole-fused pyranoxanthenone treatments shown to induce PARP-1 cleavage were tested for their ability to activate the post-mitochondrial cascade of caspases-9 and -3. Caspase-2 activity was also assayed because activation of this apical caspase may be required to activate the downstream cascade of other initator and effector caspases in drug-treated HL-60 cells (12, 14). The hypothesis that the caspase activation cascade is involved in PARP-1 cleavage by the pyrazole-fused pyranoxanthenone derivatives at 12 h is substantiated by the fact that caspase-2, -9 and -3 activities were all maximally induced by **7**, **8** and **10** after 9 h in the HL-60 cells (Figure 8). Interestingly, the concentration-dependent abilities of **7** to maximally induce caspase-2 (400% of the control), -9 (290% of the control) and -3 activities (627% of the control) in HL-60 cells at 9 h resemble the induction of internucleosomal DNA fragmentation caused by this drug at 24 h (Figures 5A and 6). The activations of these initiator and effector caspases started at 1.6 to 4 μM, increased up to peaks at 25 μM and then declined towards or even below the control levels at the higher 62.5 μM concentration of **7**, which might be too toxic to sustain the active process of apoptosis (Figure 8A). Incidentally, the ability of **10** to induce caspase-2, -9 and -3 activities at 25 μM was substantially less than that of 25 μM **7** (Figure 8B), consistent with the submaximal effect of 25 μM **10** since the induction of apoptotic DNA fragmentation peaked at 10 μM **10** and 25 μM **7** before declining thereafter (Figure 5).

*Induction of Cyt c release.* Because the release of Cyt *c* from the mitochondrial IMS into the cytosol may be a limiting factor in caspase-9 activation and represents a central coordinating step in apoptosis (16, 25), the pyrazole-fused pyranoxanthenones that activate the caspase proteolytic cascade were tested for their ability to trigger Cyt *c* release in the HL-60 cells. As compared to the untreated controls, the 15-kDa bands of cytosolic Cyt *c* became increasingly visible 3 to 6 h after 25 μM **7** and **10** treatments (data not shown) but were fully developed at 9 h, a time which was selected to determine the concentration dependency of these effects (Figure 9). Under this condition, 4 to 10 μM **7** and **10** became increasingly effective at triggering the release of Cyt *c*, which was maximally

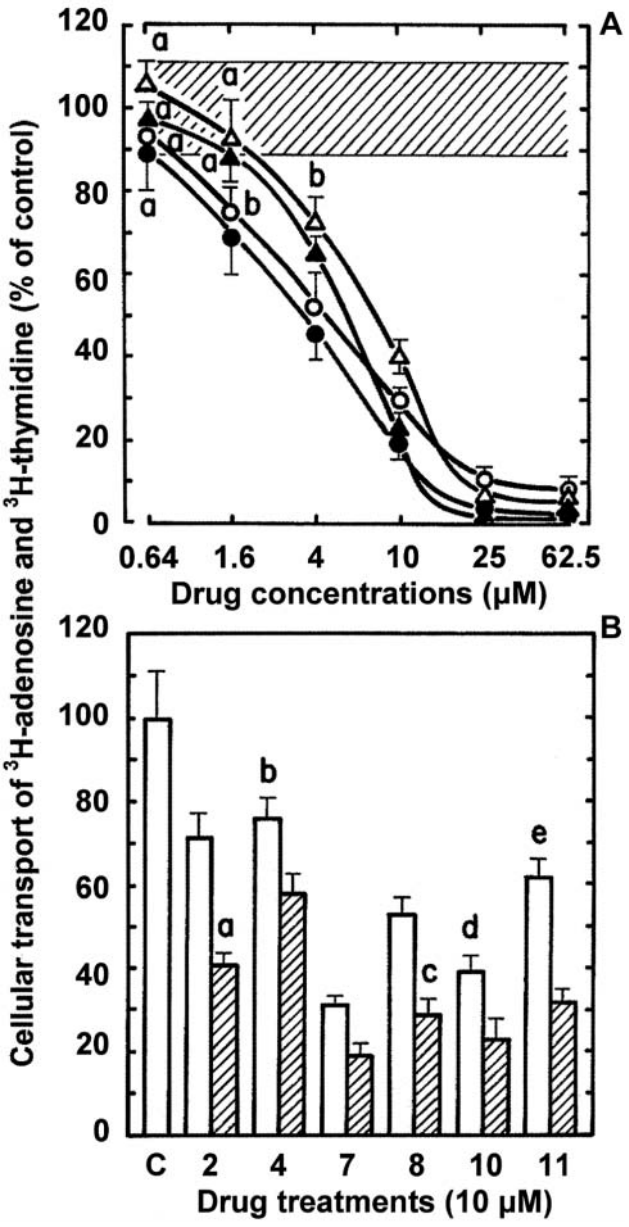


Figure 4. *Pyranoxanthenones, pyranothioxanthenones and their pyrazole-fused derivatives inhibited the cellular uptake of purine and pyrimidine nucleosides in HL-60 cells. A) Comparison of the abilities of serial concentrations (plotted on a logarithmic scale) of* ***7*** *(○,●) and* ***10*** *(△,▲) to inhibit the uptake of $^3$H-adenosine (open symbols) and $^3$H-thymidine (closed symbols) into HL-60 cells measured over 30 sec following a 15-min period of incubation at 37˚C in vitro. The results are expressed as % of $^3$H-adenosine (8.826±989 cpm) or $^3$H-thymidine (16.231±1.753 cpm) transported into vehicle-treated control cells over 30 sec (100±11%, striped area). Bars: means±SD (n=3). [a]Not different from control; [b]p<0.025, less than control. B) Comparison of the abilities of 15-min treatments with 10 μM* ***2***, ***4***, ***7***, ***8***, ***10*** *and* ***11*** *to inhibit the uptake of $^3$H-adenosine (open columns) or $^3$H-thymidine (striped columns) into HL-60 cells over 30 sec. C: control (100±11%). [a]p<0.005, less than* ***4*** *but p<0.025, more than* ***11***; *[b]p<0.025, less than control but not different from* ***2***; *[c]not different from* ***10*** *and* ***11*** *but p<0.025, more than* ***7***; *[d]p<0.025, less than* ***8*** *but p<0.05, more than* ***7***; *[e]not different from* ***2*** *but p<0.025, less than* ***4*** *and p<0.05, more than* ***8****.*

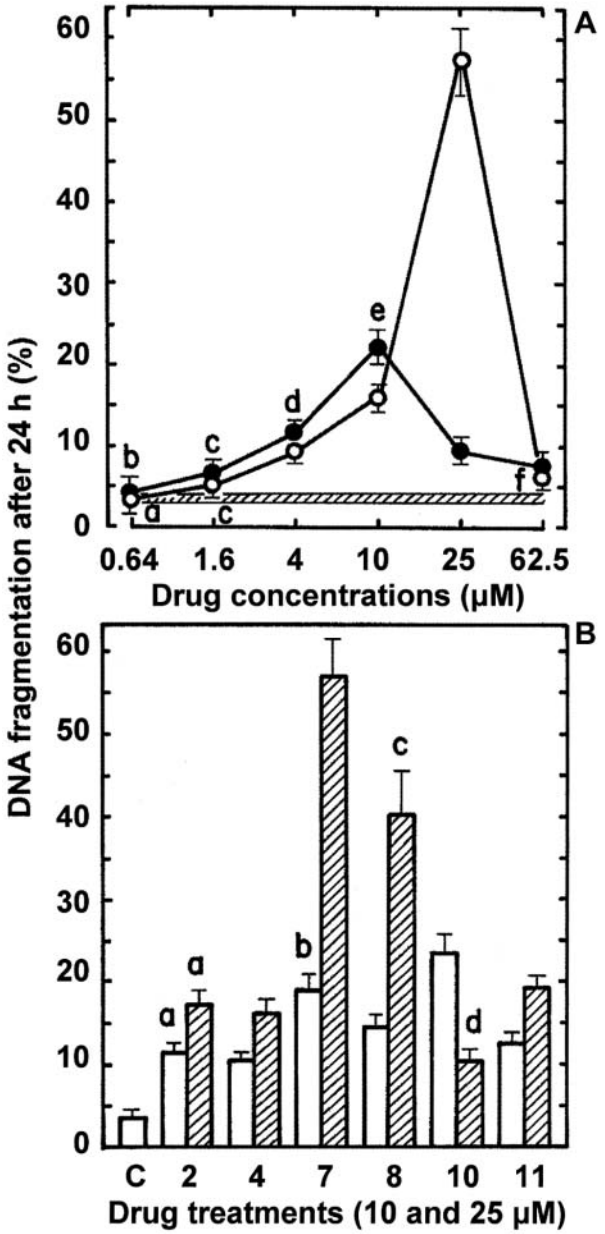


Figure 5. *Pyranoxanthenones, pyranothioxanthenones and their pyrazole-fused derivatives induced DNA fragmentation in HL-60 cells. A) Comparison of the abilities of serial concentrations (plotted on a logarithmic scale) of* ***7*** *(○) and* ***10*** *(●) to induce DNA fragmentation at 24 h in HL-60 cells containing $^3$H-prelabeled DNA in vitro. The results are expressed as [cpm in supernatant/cpm in supernatant + pellet] x 100 at 24 h. For untreated control tumor cells (3.8±0.5% DNA fragmentation, striped area), the supernatant (DNA fragments) was 4.506±622 cpm and the pellet (intact DNA) was 113.761±16.154 cpm. Bars: means±SD (n=3). [a]Not different from control; [b]not different from control and* ***7***; *[c]p<0.025, more than control but not different from* ***10***; *[d]p<0.05 and [e]p<0.025, more than* ***7***; *[f]not different from* ***10*** *but p<0.01, more than control. B) Comparison of the abilities of 10 (open columns) and 25 μM (striped columns) concentrations of* ***2***, ***4***, ***7***, ***8***, ***10*** *and* ***11*** *to induce DNA fragmentation in HL-60 cells at 24 h. C: control (3.8±0.5% DNA fragmentation). [a]Not different from* ***4*** *and* ***11***; *[b]p<0.05, more than* ***8*** *but less than* ***10***; *[c]p<0.025, less than* ***7***; *[d]p<0.0005, more than control but p<0.025, less than* ***4****.*

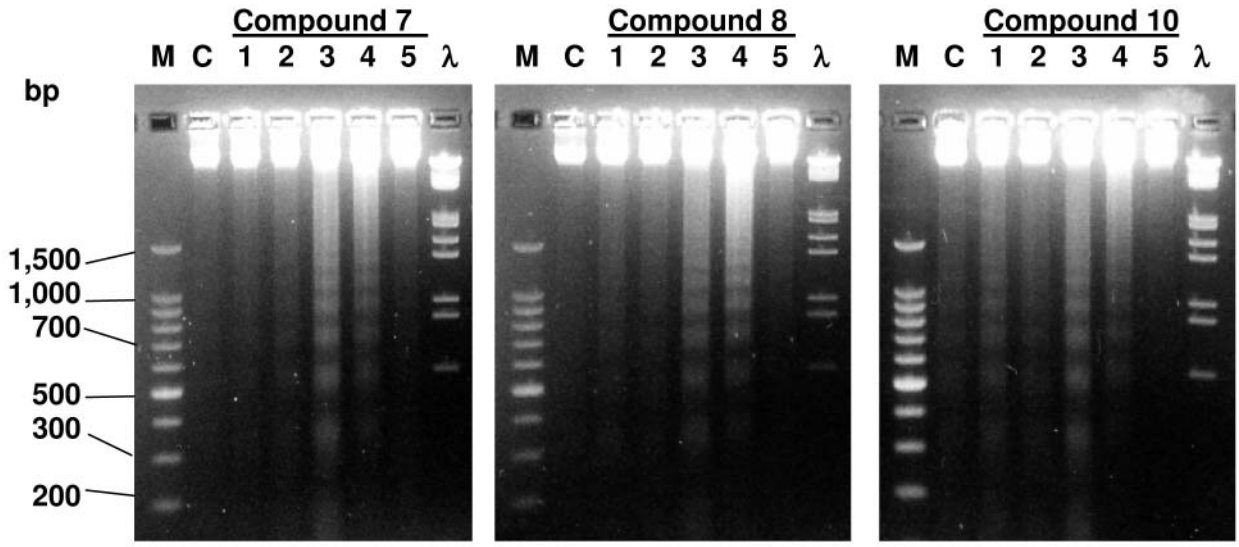


Figure 6. *Agarose gel analysis of drug-induced internucleosomal DNA fragmentation in HL-60 cells in vitro. Concentration-dependent levels of DNA fragmentation in cells incubated at 37˚C for 24 h in the presence or absence (control: lanes C) of 1.6, 4, 10, 25 and 62.5 μM concentrations of the pyrazole-fused pyranoxanthenone derivatives **7**, **8** or **10** (lanes 1-5). Cellular DNA extracts (6 μg/well) were loaded onto a 1.5% agarose gel containing EB (1 μg/ml), separated by electrophoresis for 3.7 h at 60 V and photographed under UV light. A typical ladder pattern indicating the presence of DNA equivalent to the size of single and oligo nucleosomes is characteristic of apoptosis. Size markers are shown in lanes M (0.5 μg of 100 bp standard DNA ladder) and λ (0.75 μg of lambda DNA/EcoRI + HindIII markers).*

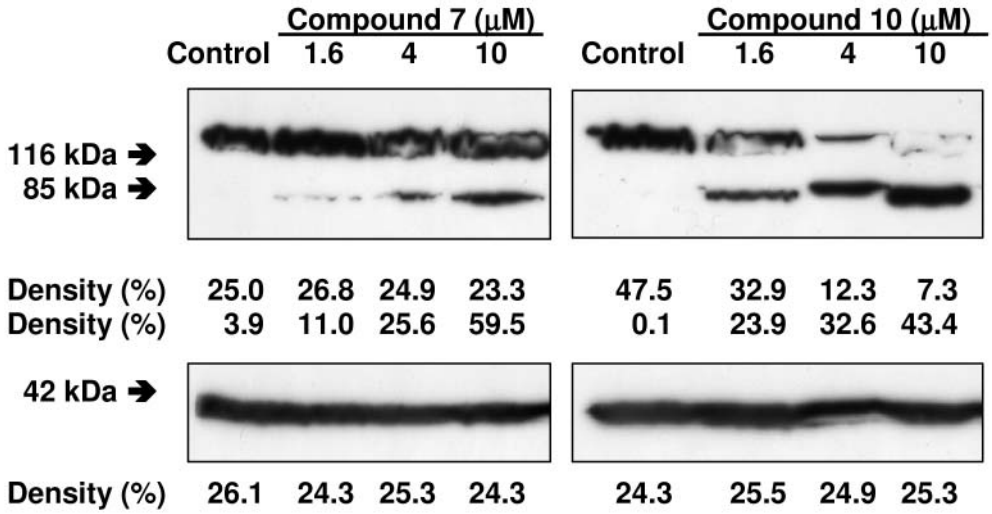


Figure 7. *Comparison of the concentration-dependent inductions of PARP-1 cleavage by pyrazole-fused pyranoxanthenone derivatives in HL-60 cells in vitro. Tumor cells were incubated for 12 h in the presence or absence (control) of 1.6 to 10 μM concentrations of **7** or **10** and bands (arrows) of intact (Mr ~ 116,000) and cleaved (Mr ~ 85,000) PARP-1 were detected by Western blot analysis. Coimmunodetection of β-actin bands (Mr ~ 42,000) was performed on the same membranes to confirm equal protein loading in each lane. The relative band densities in equal areas are expressed as the percentage that each box contributed to the total density measured after automatic background correction.*

stimulated in response to 25 μM concentrations of these compounds, as evidenced by the dense 15-kDa bands of Cyt *c* extracted from the cytosol of **7**- and **10**-treated HL-60 cells at 9 h (Figure 9).

*Mitochondrial depolarization and swelling.* Since opening of the mitochondrial PTP may be linked to ↓Δψm, large amplitude swelling and the release of apoptogenic proteins from the IMS, it was of interest to determine whether the pyrazole-fused pyranoxanthenones that trigger Cyt *c* release could target mitochondria in cell and cell-free systems to induce these markers of MPT. Treatments with 4 and 10 μM concentrations of the anticancer drug AQ9, which, on an equimolar basis, were shown to rapidly trigger ↓Δψm even

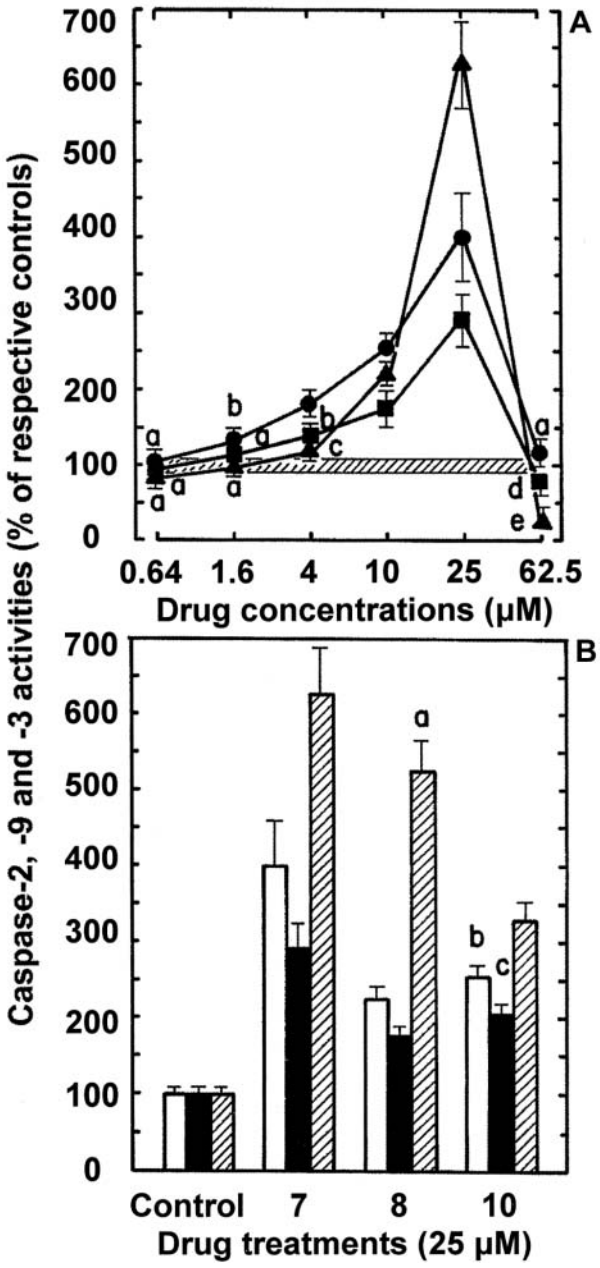


Figure 8. *Pyrazole-fused pyranoxanthenone derivatives activated initiator and effector caspases in HL-60 cells. A) Comparison of the abilities of serial concentrations (plotted on a logarithmic scale) of* ***7*** *to induce caspase-2- (●), caspase-9- (■) and caspase-3-like (▲) protease activities after 9 h in HL-60 cells in vitro. The results are respectively expressed as a % of VDVAD (30.70±2.70 nmol AFC released/mg protein), LEHD (11.26±1.01 nmol AFC released/mg protein) or DEVD (12.42±1.14 nmol AFC released/mg protein) cleavage activities in vehicle-treated control tumor cells at 9 h (100±9%, striped area). Bars: means±SD (n=3).* [a]*Not different from control;* [b]$p<0.025$ *and* [c]$p<0.05$*, more than control;* [d]$p<0.05$ *and* [e]$p<0.0005$*, less than control. B) Comparison of the abilities of 25 μM concentrations of* ***7****,* ***8*** *and* ***10*** *to induce caspase-2- (open columns), caspase-9- (closed columns) and caspase-3-like (striped columns) protease activities after 9 h in HL-60 cells in vitro.* [a]$p<0.005$*, more than* ***10*** *but not different from* ***7****;* [b]*not different from* ***8*** *but* $p<0.025$*, less than* ***7****;* [c]$p<0.05$*, more than* ***8*** *but* $p<0.025$*, less than* ***7****.*

more effectively than 10 and 25 μM concentrations of the reference depolarizing agent CCCP (13), were used as positive controls in the JC-1 assay of Δψm with HL-60 cells (Figure 10A). However, 10 to 25 μM concentrations of **7**, **8** and **10** all failed to mimic the ↓Δψm caused by CCCP and AQ9 in HL-60 cells at 40 min, suggesting that these antitumor drugs were unlikely to target mitochondria *in situ* and rapidly induce MPT (Figure 10A).

At 5 μg/ml, the transmembrane channel-forming peptide alamethicin, which functions as an uncoupler of mitochondrial oxidative phosphorylation by dissipating electrochemical gradients across the IM, directly caused a rapid and massive ↓Δψm (13) and was used as a positive control in the Rh 123 assay of Δψm with freshly isolated mitochondria (Figure 10B). Since the open-closed transition of the PTP is $Ca^{2+}$-sensitive (26, 27) and mitochondrial $Ca^{2+}$ overload triggers PTP opening, IM permeabilization, ↓Δψm, swelling and apoptosis, raising the exogenous concentration of $Ca^{2+}$ from a low of 20 μM, which has no effect on its own, to a high of 100 μM immediately induced the ↓Δψm (13) for this concentration of isolated mitochondria in suspension (0.5 mg protein/ml) (Figure 10B). Interestingly, 1.6 and 4 μM concentrations of AQ9 were inactive alone, requiring the presence of 20 μM $Ca^{2+}$ in order to induce the same ↓Δψm in isolated mitochondria at 30 min as those caused by alamethicin or 100 μM $Ca^{2+}$ (13). Thus, the antitumor AQ9 may be used as a positive control to characterize drugs that interact with the PTP to induce conformational changes that increase its $Ca^{2+}$ sensitivity, so that the low and normally ineffective 20 μM concentration of exogenous $Ca^{2+}$ became sufficient to prime PTP opening (Figure 10B). However, 10 to 25 μM **7**, **8** and **10** were totally unable to induce a significant ↓Δψm in isolated mitochondria incubated for 30 min in the presence of 20 μM $Ca^{2+}$ primer, suggesting that these pyrazole-fused pyranoxanthenone derivatives cannot directly target these organelles in a cell-free system to interact with, and increase the $Ca^{2+}$ sensitivity of the PTP (Figure 10B).

Finally, the hypothesis that **7**, **8** and **10** cannot directly target mitochondria to trigger PTP opening and the $Ca^{2+}$-dependent induction of ↓Δψm was substantiated by the fact that these pyrazole-fused pyranoxanthenone derivatives also failed to mimic the large amplitude swelling truly indicative of MPT caused by alamethicin, 100 μM $Ca^{2+}$ overload or antitumor AQ9 in the presence of a 20 μM $Ca^{2+}$ primer in isolated mitochondria within 30 min (Figure 10C).

## Discussion

In agreement with the report that incorporation of an amino-substituted pyrazole ring into the acronycine chromophore, or into its isosteres, improved the bioactivity of the lead compounds (6), the present study confirmed that the pyranoxanthenones and pyranothioxanthenones have less

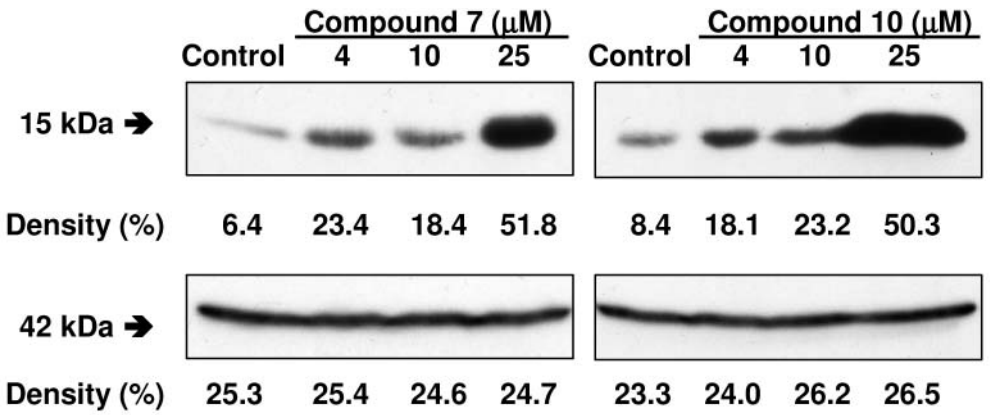


Figure 9. *Comparison of the concentration-dependent inductions of Cyt c release by pyrazole-fused pyranoxanthenone derivatives in HL-60 cells in vitro. Tumor cells were incubated for 9 h in the presence or absence (control) of 4 to 25 μM concentrations of* ***7*** *or* ***10*** *and bands (arrows) of cytosolic Cyt c (Mr ~ 15,000) released from the mitochondrial IMS were detected by Western blot analysis. Coimmunodetection of β-actin bands (Mr ~ 42,000) was performed on the same membranes to confirm equal protein loading in each lane. The relative band densities in equal areas are expressed as the percentage that each box contributes to the total density measured after automatic background correction.*

antitumor activity in the HL-60 cell system than their pyrazole-fused derivatives. The cytotoxicity of these compounds was not improved by a methoxy substitution or by switching from an O to a S to replace the N atom of acronycine, but the side chain was more effective with $N(CH_2)_4$ than $N(CH_2)_5$. Some acronycine analogs have a broad spectrum of *in vitro* and *in vivo* antitumor activities against several ascitic and solid tumor cells of murine or human origins, including a panel of MDR sublines, but their molecular targets and mechanisms of action have not been fully investigated (2, 28-34). This new class of compounds displayed solid tumor selectivity, and was more cytotoxic towards solid tumor cells than leukemia or normal cells (29, 30). Because their planar polycyclic chromophore can intercalate into DNA and their basic side chain(s) may increase their DNA binding affinity, antitumor acronycine derivatives are generally potent DNA-interacting agents, although DNA intercalation may be required, but not sufficient, for their antitumor activity (29, 30). Like the insecticidal chromene precocenes that act on mitochondrial and nuclear membranes, acronycine derivatives have been suggested to alter the surface components of membranous organelles (32). Pyrazole-fused pyranoxanthenone derivatives are, however, unlikely to directly target mitochondria and disrupt components of the PTP complex since they are unable to rapidly induce large amplitude swelling in isolated mitochondria and ↓$\Delta\psi m$ in cell and cell-free systems.

As compared to acronycine, which blocks cell cycle progession in the $G_2$ + M-phases, 1,2-dihydro-1,2-dihydroacronycine diesters and benzo[*b*]pyrano[3,2-*h*]acridin-7-one analogs of acronycine had higher antitumor potency against L1210 cells *in vitro* and P388 leukemia and colon 38 adenocarcinoma *in vivo* and induced tumor cell accumulation in the S-phase after 21 h, suggesting that these compounds have different molecular mechanisms of action (32, 34). Blocking cell cycle progression in the S-phase is characteristic of inhibitors of nucleic acid synthesis and is consistent with the observation that all the compounds tested in the present study inhibited DNA synthesis at 2 h in relation to their ability to block the cellular uptake of purine and pyrimidine nucleosides at 15 min and the proliferation of HL-60 cells at 2 and 4 days. Some of the same pyranoxanthenone and pyrano-thioxanthenone structures were also shown to block tumor cell cycle progression in the $G_2$ + M-phases like acronycine (5), suggesting that, in addition to blocking nucleoside transporters and DNA synthesis, these DNA-interacting agents are likely to disrupt other molecular targets in order to arrest the transition of damaged and possibly apoptotic tumor cells at various cell cycle checkpoints 21 h later. Unrepairable and cytotoxic DNA-strand breaks might be involved since various hycanthone derivatives, which differ in their pyrazolo ring fusion and phenolic hydroxy substitution, have similar DNA-binding and intercalative activities, but inhibit P388 cell viability *in vitro* compared to their effectiveness as inhibitors of DNA topoisomerase II (33).

In contrast to the early cleavage of DNA into large 50 to 300-kbp fragments, an initial signaling event that may induce tumor cells treated with relatively low concentrations of DNA-damaging anticancer drugs to commit apoptosis, the secondary endonucleolytic degradation of DNA at internucleosomal linker sites to produce small 180 to 200-bp mono- and oligonucleosomal fragments at 24 h is a late marker concurrent with morphological evidence of apoptosis (9, 35). Upstream of internucleosomal DNA fragmentation, activation of the caspase cascade induces the proteolytic cleavage of a wide range of substrates. Effector caspase-3 cleaves and inactivates the inhibitor of caspase-activated DNase, thus releasing active endonucleases that translocate into the nucleus to achieve internucleosomal DNA fragmentation (9, 35). The caspase-3-mediated cleavage and inactivation of PARP-1 is also an early

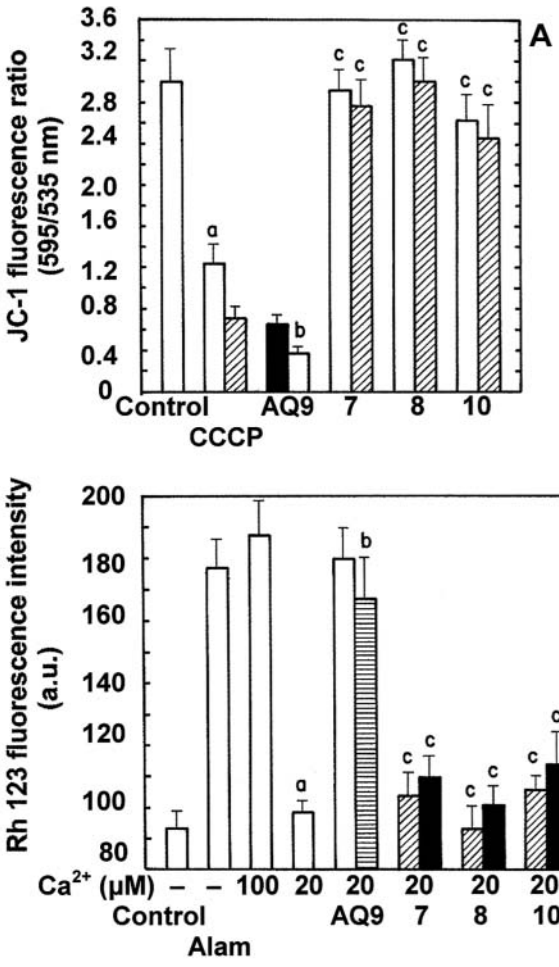


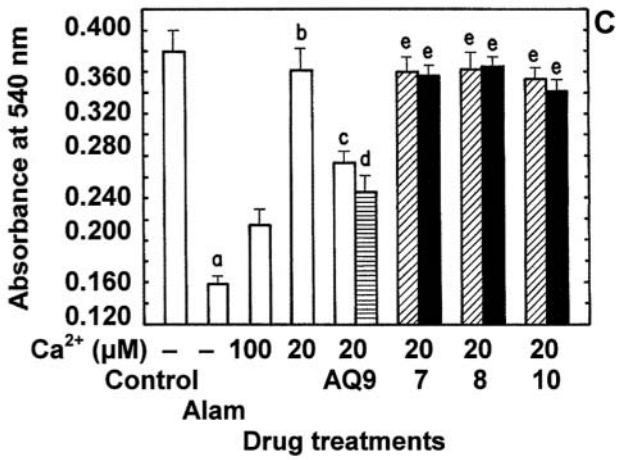


Figure 10. *Pyrazole-fused pyranoxanthenone derivatives did not induce mitochondrial ↓Δψm and swelling in cell and cell-free systems. A) Comparison of the abilities of 4 (closed column), 10 (open columns) or 25 μM (striped columns) concentrations of* ***7, 8, 10*** *and the reference depolarizing agents CCCP and AQ9 to decrease the red:green fluorescence ratio of JC-1 aggregates:monomers indicating the ↓Δψm after 40 min in HL-60 cells in vitro. JC-1 was loaded for the last 30 min of incubation. Control: JC-1 fluorescence ratio in non-treated cells (3.05±0.32). Bars: means±SD (n=3).* $^{a}p<0.005$*, less than control;* $^{b}p<0.01$*, less than 25 μM CCCP;* $^{c}$*not different from control. B) Comparison of the abilities of 5 μg/ml alamethicin (Alam), 20 or 100 μM* $CaCl_2$*, and 1.6 (open column), 4 (horizontal stripes), 10 (diagonal stripes) or 25 μM (solid columns) concentrations of AQ9,* ***7, 8*** *and* ***10,*** *in the presence of a 20 μM* $Ca^{2+}$ *primer, to directly induce the ↓Δψm in isolated mitochondria, based on the unquenched fluorescence (arbitrary units) of Rh 123 released from these drug-treated organelles at 30 min. Control: Rh 123 fluorescence intensity in non-treated suspensions of isolated mitochondria (93.8±5.6). Bars: means±SD (n=3).* $^{a}$*Not different from control;* $^{b}p<0.005$*, more than 20 μM* $Ca^{2+}$*;* $^{c}$*not different from 20 μM* $Ca^{2+}$*. C) Comparison of the abilities of 5 μg/ml alamethicin (Alam), 20 or 100 μM* $CaCl_2$*, and 1.6 (open column), 4 (horizontal stripes), 10 (diagonal stripes) or 25 μM (solid columns) concentrations of AQ9,* ***7, 8*** *and* ***10,*** *in the presence of a 20 μM* $Ca^{2+}$ *primer, to directly induce the large amplitude swelling of isolated mitochondria, based on the decrease in absorbance (light scattering) at 540 nm that occured after 30 min in severely swollen organelles with diluted matrices and disrupted cristae. Control: absorbance at 540 nm of non-treated suspensions of isolated mitochondria (0.380±0.019). Bars: means±SD (n=3).* $^{a}p<0.005$*, less than 100 μM* $Ca^{2+}$*;* $^{b}$*not different from control;* $^{c}p<0.005$*, less than 20 μM* $Ca^{2+}$ *but* $p<0.05$*, more than 4 μM AQ9;* $^{d}p<0.05$*, more than 100 μM* $Ca^{2+}$*;* $^{e}$*not different from 20 μM* $Ca^{2+}$*.*

event required for tumor cells that have been exposed to DNA-damaging anticancer drugs and have entered the process of apoptosis. PARP-1 cleavage may prevent the detection and repair of DNA damage, block the depletion of $NAD^+$ and ATP causing necrotic cell death and enhance the activity of $Ca^{2+}/Mg^{2+}$-dependent endonucleases (24, 36). For this reason, detection of the disappearance of the native 116-kDa enzyme and appearance of the 85-kDa fragment of PARP-1 cleavage is an early and sensitive indicator that HL-60 cells treated with pyrazole-fused pyranoxanthenone derivatives are undergoing apoptosis (11, 12). The present data indicated that low μM concentrations of **7** and **10**, which blocked nucleoside transport at 15 min and inhibited DNA synthesis within 2 h, triggered an apoptotic pathway that induced Cyt *c* release and postmitochondrial caspase activation at 9 h and PARP-1 cleavage at 12 h in relation to their ability to decrease HL-60 tumor cell proliferation over a 2 to 4-day period, suggesting that the ability of these pyrazole-fused pyranoxanthenones to induce apoptosis may play a significant role in their molecular mechanism of action. Since apoptosis is an active ATP-driven and cell cycle phase-specific process that requires the expression of specific genes, the synthesis of new RNA and proteins and the activation of caspases, non-caspase proteases and nucleases, inhibition of such mechanisms can prevent apoptotic DNA fragmentation (11, 15). Hence, the fact that the concentration-dependent inductions of caspase-2, -9 and -3 activities and internucleosomal DNA fragmentation by **7** and **10** in HL-60 cells are similarly biphasic suggests that, even though they are increasingly cytostatic, higher concentrations of pyrazole-fused pyranoxanthenone derivatives may inhibit DNA and other macromolecule syntheses to such excessive

degrees and be so cytotoxic as to abolish their own ability to sustain the active process of apoptosis induced by low μM concentrations of these compounds (12, 14).

Since the abilities of pyrazole-fused pyranoxanthenone derivatives to inhibit DNA topoisomerase activities and cause high molecular weight DNA-strand breaks and crosslinks remain to be determined, it is rather premature to speculate on the nature of the primary molecular targets and massive damaging events that induce **7**- and **10**-treated HL-60 cells to commit apoptosis. Cyt *c* release is a universal event in apoptosis but this can occur before, independently of, or in the absence of ↓$\Delta\psi$m and without concomitant mitochondrial PTP opening and swelling (13). Since **7** and **10** did not cause mitochondrial ↓$\Delta\psi$m or swelling in cell and cell-free systems, any rapid mitochondrial interaction of these compounds to cause Cyt *c* release can be ruled out, either directly, through conformational changes that disrupt the open-closed transition of the PTP complex (26, 27), or indirectly, through sequential DNA damage and early PARP-1 activation resulting in mitochondrial $NAD^+$ depletion and dysfunction (37). However, rapid, massive and unrepairable DNA damage secondary to topoisomerase inhibition might be the trigger initiating nuclear signals that induced **7**- and **10**-treated tumor cells to release their mitochondrial Cyt *c* and undergo apoptosis, thereby activating their postmitochondrial caspase cascade responsible for PARP-1 cleavage, endonuclease activation and, ultimately, the internucleosomal fragmentation of their DNA, one of the late manifestations of the apoptotic process (35, 38).

The Fas ligand and death receptor systems that signal an extrinsic pathway involving the caspase-8-mediated cleavage of Bid do not appear to be required for the mechanism of anticancer drug-induced apoptosis (12, 14). Truncated Bid facilitates the insertion and oligomerization of Bax and Bak into the mitochondrial outer membrane where these pro-apoptotic Bcl-2 family members trigger MPT and Cyt *c* release. In contrast, DNA-damaging anticancer drugs are believed to trigger an intrinsic mitochondrial-dependent pathway in which nuclear-mediated signals, that may involve various p53-responsive genes, directly induce the Bax- and Bak-mediated opening of the mitochondrial pores and the release of Cyt *c* (25). In any case, all apoptotic pathways eventually converge on the mitochondria and the release of Cyt *c* from the IMS into the cytosol, which is the key limiting factor in initiating the postmitochondrial cascade of apoptotic proteases (8, 9). Cyt *c* binds to apoptotic protease-activating factor-1 which, through its caspase recruitment domain, interacts with procaspase-9, resulting in the formation of the apoptosome complex that activates this initiator caspase in the presence of dATP (16, 25). In drug-treated HL-60 cells, the critical release of mitochondrial Cyt *c* can occur in the absence of apical caspase activation, suggesting that Cyt *c* release is an upstream and caspase-independent event in drug-induced apoptosis (12, 14). However, a specific caspase-2 inhibitor blocks caspase-9, -3 and -8 activations in drug-treated HL-60 cells, demonstrating that apical caspase-2 may be activated upstream of the other initiator and effector caspases and control their subsequent activations (12, 14). Whatever apoptosis signaling pathways may be involved in the mechanisms by which **7** and **10** triggered mitochondrial Cyt *c* release, initiator and effector caspase activation, PARP-1 cleavage and internucleosomal DNA fragmentation in HL-60 cells, they are definitively *p53*-independent since p53 is not expressed in an active form in these p53-null tumor cells (12, 14).

## Acknowledgements

This study was supported by grants from the National Institutes of Health (National Cancer Institute CA86842 and Center of Biomedical Research Excellence RR15563, with matching funds from the State of Kansas), the Howard Hughes Medical Institute (Biological Sciences Education Grant) and Kansas State University (Terry C. Johnson Center for Basic Cancer Research), USA.

## References

1 Scarffe JH, Beaumont AR and Crowther D: Phase I-II evaluation of acronycine in patients with multiple myeloma. Cancer Treat Rep *67*: 93-94, 1983.

2 Dorr RT, Liddil JD, Von Hoff DD, Soble M and Osborne CK: Antitumor activity and murine pharmacokinetics of parenteral acronycine. Cancer Res *49*: 340-344, 1989.

3 Shieh H-L, Pezzuto JM and Cordell GA: Evaluation and cytotoxic mechanisms mediated by the broad- spectrum antitumor alkaloid acronycine and selected semisynthetic derivatives. Chem-Biol Interact *81*: 35- 55, 1992.

4 Tillequin F, Michel S and Skaltsounis A-L: Acronycine-type alkaloids: chemistry and biology. *In*: Alcaloids: Chemical and Biological Perspectives. Pelletier SW (ed.). Amsterdam, Elsevier, Vol. 12, pp. 1-102, 1998.

5 Kostakis I, Ghirtis K, Pouli N, Marakos P, Skaltsounis A-L, Leonce S, Caignard DH and Atassi G: Synthesis and cytotoxic activity of 2-dialkylaminoethylamino substituted xanthenone and thioxanthenone derivatives. Il Farmaco *55*: 455-460, 2000.

6 Kostakis IK, Magiatis P, Pouli N, Marakos P, Skaltsounis A-L, Pratsinis H, Léonce S and Pierré A: Design, synthesis, and antiproliferative activity of some new pyrazole-fused amino derivatives of the pyranoxanthenone, pyranothioxanthenone, and pyranoacridone ring systems: a new class of cytotoxic agents. J Med Chem *45*: 2599-2609, 2002.

7 Judson IR: Anthrapyrazoles: true successors to the anthracyclines? Anti-Cancer Drugs *2*: 223-231, 1991.

8 Budihardjo I, Oliver H, Lutter M, Luo X and Wang X: Biochemical pathways of caspase activation during apoptosis. Annu Rev Cell Dev Biol *15*: 269-290, 1999.

9 Nagata S: Apoptotic DNA fragmentation. Exp Cell Res *256*: 12-18, 2000.

10 Wu M, Wang B, Perchellet EM, Sperfslage BJ, Stephany HA, Hua DH and Perchellet J-P: Synthetic 1,4- anthracenediones, which block nucleoside transport and induce DNA fragmentation, retain their cytotoxic efficacy in daunorubicin-resistant HL-60 cell lines. Anti-Cancer Drugs *12*: 807-819, 2001.

11 Wang Y, Perchellet EM, Tamura M, Hua DH and Perchellet J-P: Induction of poly(ADP-ribose) polymerase-1 cleavage by antitumor triptycene bisquinones in wild-type and daunorubicin-resistant HL-60 cell lines. Cancer Lett *188*: 73-83, 2002.

12 Perchellet EM, Wang Y, Weber RL, Sperfslage BJ, Lou K, Crossland J, Hua DH and Perchellet J-P: Synthetic 1,4-anthracenedione analogs induce cytochrome *c* release, caspase-9, -3, and -8 activities, poly(ADP-ribose) polymerase-1 cleavage and internucleosomal DNA fragmentation in HL-60 cells by a mechanism which involves caspase-2 activation but not Fas signaling. Biochem Pharmacol *67*: 523-537, 2004.

13 Wang Y, Perchellet EM, Ward MM, Lou K, Hua DH and Perchellet J-P: Rapid collapse of mitochondrial transmembrane potential in HL-60 cells and isolated mitochondria treated with anti-tumor 1,4- anthracenediones. Anti-Cancer Drugs *16*: 953-967, 2005.

14 Perchellet EM, Wang Y, Weber RL, Lou K, Hua DH and Perchellet J-P: Antitumor triptycene bisquinones induce a caspase-independent release of mitochondrial cytochrome *c* and a caspase-2-mediated activation of initiator caspase-8 and -9 in HL-60 cells by a mechanism which does not involve Fas signaling. Anti-Cancer Drugs *15*: 929-946, 2004.

15 Perchellet EM, Sperfslage BJ, Wang Y, Huang X, Tamura M, Hua DH and Perchellet J-P: Among substituted 9,10-dihydro-9,10-[1,2]benzenoanthracene-1, 4, 5, 8-tetraones, the lead antitumor triptycene bisquinone TT24 blocks nucleoside transport, induces apoptotic DNA fragmentation and decreases the viability of L1210 leukemic cells in the nanomolar range of daunorubicin *in vitro*. Anti-Cancer Drugs *13*: 567-581, 2002.

16 Liu X, Kim CN, Yang J, Jemmerson R and Wang X: Induction of apoptotic program in cell-free extracts: requirement for dATP and cytochrome *c*. Cell *86*: 147-157, 1996.

17 Reers M, Smith TW and Chen LB: J-aggregate formation of a carbocyanine as a quantitative fluorescent indicator of membrane potential. Biochemistry *30*: 4480-4486, 1991.

18 Cossarizza A, Baccarani-Contri M, Kalashnikova G and Franceschi C: A new method for the cytofluorimetric analysis of mitochondrial membrane potential using the J-aggregate forming lipophilic cation 5,5',6,6'- tetrachloro-1,1',3,3'-tetraethylbenzimidazolcarbocyanine iodide (JC-1). Biochem Biophys Res Commun *197*: 40-45, 1993.

19 Susin SA, Larochette N, Geuskens M and Kroemer G: Purification of mitochondria for apoptosis assays. Methods Enzymol *322*: 205-208, 2000.

20 Blattner JR, He L and Lemasters JJ: Screening assays for the mitochondrial permeability transition using a fluorescence multiwell plate reader. Anal Biochem *295*: 220-226, 2001.

21 Emaus RK, Grunwald R and Lemasters JJ: Rhodamine 123 as a probe of transmembrane potential in isolated rat-liver mitochondria: spectral and metabolic properties. Biochim Biophys Acta *850*: 436-448, 1986.

22 Halestrap AP: The regulation of the matrix volume of mammalian mitochondria *in vivo* and *in vitro* and its role in the control of mitochondrial metabolism. Biochim Biophys Acta *973*: 355-382, 1989.

23 Zamzami N, Maisse C, Metivier D and Kroemer G: Measurement of membrane permeability and permeability transition of mitochondria. Methods Cell Biol *65*: 147-158, 2001.

24 Duriez PJ and Shah GM: Cleavage of poly(ADP-ribose) polymerase: a sensitive parameter to study cell death. Biochem Cell Biol *75*: 337-349, 1997.

25 Li P, Nijhawan D, Budihardjo I, Srinivasula SM, Ahmad M, Alnemri ES and Wang X: Cytochrome *c* and dATP-dependent formation of Apaf-1/Caspase-9 complex initiates an apoptotic protease cascade. Cell *91*: 479-489, 1997.

26 Fontaine E, Ichas F and Bernardi P: A ubiquinone-binding site regulates the mitochondrial permeability transition pore. J Biol Chem *273*: 25734-25740, 1998.

27 Walter L, Miyoshi H, Leverve X, Bernardi P and Fontaine E: Regulation of the mitochondrial permeability transition pore by ubiquinone analogs. A progress report. Free Radical Res *36*: 405-412, 2002.

28 Schneider J, Evans EL, Grunberg E and Fryer RI: Synthesis and biological activity of acronycine analogs. J Med Chem *15*: 266-270, 1972.

29 Capps DB, Dunbar J, Kesten SR, Shillis J and Werbel LM: 2-(Aminoalkyl)-5-nitropyrazolo[3,4,5-*kl*]acridines, a new class of anticancer agents. J Med Chem *35*: 4770-4778, 1992.

30 Horwitz JP, Massova I, Wiese TE, Besler BH and Corbett TH: Comparative molecular field analysis of the antitumor activity of 9*H*-thioxanthen-9-one derivatives against pancreatic ductal carcinoma 03. J Med Chem *37*: 781-786, 1994.

31 Antonini I, Cola D, Polucci P, Bontemps-Gracz M, Borowski E and Martelli S: Synthesis of (dialkylamino)alkyl-disubstituted pyrimido[5,6,1-*de*]acridines, a novel group of anticancer agents active on a multidrug resistant cell line. J Med Chem *38*: 3282-3286, 1995.

32 Elomri A, Mitaku S, Michel S, Skaltsounis A-L, Tillequin F, Koch M, Pierré A, Guilbaud N, Léonce S, Kraus-Berthier L, Rolland Y and Atassi G: Synthesis and cytotoxic and antitumor activity of esters in the 1,2-dihydroxy-1,2-dihydroacronycine series. J Med Chem *39*: 4762-4766, 1996.

33 Perni RB, Wentland MP, Huang JI, Powles RG, Aldous S, Klingbeil KM, Peverly AD, Robinson RG, Corbett TH, Jones JL, Mattes KC, Rake JB and Coughlin SA: Synthesis and antitumor activity of 4-aminomethylthioxanthenone and 5-aminomethylbenzothiopyranoindazole derivatives. J Med Chem *41*: 3645-3654, 1998.

34 Costes N, Le Deit H, Michel S, Tillequin F, Koch M, Pfeiffer B, Renard P, Léonce S, Guilbaud N, Kraus-Berthier L, Pierré A and Atassi G: Synthesis and cytotoxic and antitumor activity of benzo[*b*]pyrano[3,2-*h*]acridin-7-one analogues of acronycine. J Med Chem *43*: 2395-2402, 2000.

35 Compton MM: A biochemical hallmark of apoptosis: internucleosomal degradation of the genome. Cancer Metastasis Rev *11*: 105-112, 1992.

36 Herceg Z and Wang ZQ: Functions of poly(ADP-ribose) polymerase (PARP) in DNA repair, genomic integrity and cell death. Mutat Res *477*: 97-110, 2001.

37 Alano CC, Ying W and Swanson RA: Poly(ADP-ribose) polymerase-1-mediated cell death in astrocytes requires $NAD^+$ depletion and mitochondrial permeability transition. J Biol Chem *279*: 18895-18902, 2004.

38 Kamesaki S, Kamesaki H, Jorgensen TJ, Tanizawa A, Pommier Y and Cossman J: Bcl-2 protein inhibits etopside-induced apoptosis through its effects on events subsequent to topoisomerase II-induced DNA strand breaks and their repair. Cancer Res *53*: 4251-4256, 1993.

*Received April 13, 2006*
*Accepted May 25, 2006*